RSC Advances

PAPER

Cite this: *RSC Adv.*, 2021, **11**, 25170

Experimental study on the degradation mechanism of $LaCoO_3$-based symmetric supercapacitors

Xu Chen,†[a] Qiwei Su,†[a] Jipan Yu,[a] Mingrui Wei,*[a] Guanlun Guo *[a] and Yun Wang*[b]

Received 29th April 2021
Accepted 7th July 2021

DOI: 10.1039/d1ra03362j

rsc.li/rsc-advances

In this paper, $LaCoO_3$ powders were prepared by the urea combustion method and used as electrode materials for supercapacitors. The effect of the potential window and the current density on the performance degradation of $LaCoO_3$ electrodes during the cycling test was analyzed. The degradation mechanism of $LaCoO_3$-based symmetric supercapacitors was discussed. The results of the cycling test show that: with the increase in potential window and current density, the performance degradation in the cycling test becomes more intense. The results of cyclic voltammetry tests, galvanostatic charge–discharge tests, X-ray photoelectron spectroscopy tests and KOH electrolyte concentration measurements before and after the cycling test show that the degradation of the supercapacitors is mainly caused by the occurrence and accumulation of irreversible redox reactions during the charge and discharge process, which reduces the ratio of Co^{2+}/Co^{3+} and the number of oxygen vacancies.

1. Introduction

Supercapacitors (SCs) are a new type of energy storage device with properties between Li-batteries and conventional capacitors. Because of their high power density, high charging/discharging rate, wide working temperature range, remarkable cycle stability and excellent reliability,[1–3] SCs are used as a promising complement or alternative to batteries for applications of high power output or fast energy harvesting, such as electric vehicles,[4–6] rail transits,[7,8] wind power generation[9] and photovoltaic generation.[10,11]

SCs are mechanically divided into electric double layer capacitors (EDLCs) and pseudocapacitors, which exhibit different advantages and disadvantages in terms of performance. EDLCs use carbon materials as electrode materials. There is only the physical electrostatic adsorption and desorption process during the energy storage process of them, and the capacitance retention is above 95% after thousands or even tens of thousands of cycles.[12–16] On the other side, pseudocapacitors mainly use metallic materials and their compounds. Metal oxides are the most common pseudocapacitor materials with excellent electrochemical properties. Metal sulfides and selenides are also of interest because of their special properties.[17–22] The energy storage process is dominated by Faraday redox reactions. Although redox reactions result in the high energy density of pseudocapacitors, they may induce the intrinsic instability of some pseudocapacitor materials that undermining the cycle stability of pseudocapacitors.[23] It means that the cycle life of pseudocapacitors is usually worse than that of EDLCs, which is a major obstacle to practical application.

Among metal oxides, perovskite-type oxides are competitive candidates for pseudocapacitor materials.[24,25] The structural stability of perovskite-type oxides makes them have high cycle stability as electrode materials, while the existence of oxygen vacancies improves their capacitance performance. That is, perovskite-type oxide may simultaneously achieve high stability and high capacitance. However, the cycle stability of many perovskite-type oxides as electrode materials is not as excellent as excepted. The specific capacitance of electrodes decreases to below 90% (ref. 26–29) or even below 80% (ref. 30–33) after thousands of cycles. The widely accepted criteria defines the end-of-life of a supercapacitor when the capacitance retention is less than 80% or the internal resistance is doubled.[34,35] The composite method is an effective way to improve the cycle stability of these electrode materials. For example, $LaNiO_3$/NiO composite[36] and LSC@MnO_2 core/shell nanorods[37] have the capacitance retention of over 95% after thousands of cycles. And how to improve the inherent cycle stability of perovskite-type oxides is also an important issue.

In terms of practicality, cycle stability is indeed a critical issue and challenge for supercapacitors. Briat *et al.* studied the ageing quantification of supercapacitors in terms of evolution of capacitance and equivalent series resistance, and proposed an online characterisation procedure to deal with the regeneration phenomenon during the rest period.[38] And they studied the performance fading of supercapacitors under calendar life and power cycling tests, and confirmed that the two types of ageing tests affected the supercapacitor performances

[a]*Hubei Key Laboratory of Advanced Technology for Automotive Components, Hubei Collaborative Innovation Center for Automotive Components Technology, Wuhan University of Technology, Wuhan 430070, China. E-mail: glguo@whut.edu.cn; weimingrui@whut.edu.cn*

[b]*Hubei University of Arts and Science, Xiangyang, 441053, China. E-mail: 1295355658@qq.com*

† These authors contributed equally to this work.

differently.[39] During the calendar life tests, deposit of impurities on the surface of the electrodes limit the access of ions to the porous structure and lead to a decrease of the capacitance. While during the power cycling tests, the impurities accumulated more inside the electrodes, which drastically modified the structure of the electrodes and degraded the homogeneity of the cells. Summarizing several studies on the life model of supercapacitors, Liu *et al.* gave a general form of different lifetime models of supercapacitors with three critical stressors of temperature, voltage and current.[40] The failure mechanisms of EDLCs include the reaction of impurities in the electrode with the electrolyte, solvent decomposition, electrolyte evaporation, electrolyte ions intercalation into and damaging the electrode. Julien *et al.* reported that the two main causes for degradation of MnO^{2-} based pseudocapacitors are Mn^{3+} generation during the redox process and Mn^{2+} dissolution in the electrolyte.[41] And similar to EDLCs, the electrolyte decomposition and evaporation under harsh conditions also lead to the failure of pseudocapacitors.[42]

$LaCoO_3$ is a typical perovskite-type oxide. Guo *et al.* reported that the etched $LaCoO_3$ exhibits high capacitance performance as electrode material and the $LaCoO_3$//GO device shows excellent cycling performance.[43] Nevertheless, it is still necessary to study and discuss the cycle stability of $LaCoO_3$ electrodes. In this paper, in order to study the degradation of $LaCoO_3$ more accurately and eliminate the influence of GO electrodes, $LaCoO_3$-based symmetric supercapacitors are taken as the research object. The effect of potential window and current density on the performance degradation of devices is studied through the cycling test. By analyzing the changes of electrochemical performance, material element valence distribution and electrolyte composition before and after the test, the degradation mechanism of devices is obtained. Results show that the occurrence and accumulation of irreversible redox reactions reduce the number of oxygen vacancies in $LaCoO_3$ electrodes then lead to the performance degradation of the pseudocapacitors.

2. Experimental section

2.1 Preparation and characterization of $LaCoO_3$ powders

$LaCoO_3$ powders were prepared by urea combustion method[44] in this work. The phase analysis of prepared samples were carried out by X-ray diffraction (XRD, Bruker D8 Advance) in a 2θ range of 20–80° with Cu Kα radiation. The specific surface area and pore size distribution of the samples were characterized by Brunauer–Emmett–Teller (BET, Micromeritics ASAP 2020 HD88) measurements. The morphology and microstructure of the samples were examined by field emission scanning electron microscopy (FESEM, Zeiss Ultra Plus). The crystal structure was characterized by transmission electron microscopy (TEM, JEOL JEM 2100), including energy dispersive spectroscopy (EDS) and selected area electron diffraction (SAED) analysis. The chemical composition on the surface of the samples was determined by X-ray photoelectron spectroscopy (XPS, ESCALAB 250xi).

2.2 Electrochemical measurements

Electrochemical measurements were performed for $LaCoO_3$ electrodes and $LaCoO_3$-based symmetric supercapacitors in a three-electrode system and a two-electrode system, respectively, to study the factors and mechanism of their degradation. $LaCoO_3$ electrodes were prepared by pasting the mixture of $LaCoO_3$, polyvinylidene fluoride and acetylene black at the mass ratio of 8 : 1 : 1 on the nickel foam and pressing at 10 MPa. $LaCoO_3$ samples were used as active materials, polyvinylidene fluoride was used as binder and acetylene black was used as conductive agent. In the three-electrode system, prepared $LaCoO_3$ electrodes were used as the working electrodes, platinum wires were used as the counter electrodes and Hg/HgO electrodes were used as the reference electrodes. In the two-electrode system, $LaCoO_3$ electrodes were connected to the working electrodes as positive electrodes, and connected to the counter and reference electrodes simultaneously as negative electrodes. 6 M KOH was used as electrolyte in the two test systems. Three electrochemical measurements, namely cyclic voltammetry (CV) test, galvanostatic charge–discharge (GCD) tests and cyclic charge–discharge test, were carried out utilizing an electrochemical workstation CS150 (Corrtest Co. Ltd Wuhan). The specific capacitance was calculated from GCD curves according to the following equation.[24]

$$C = \frac{I\Delta t}{m\Delta V} \quad (1)$$

where I is the discharge current, Δt is the discharge time, m is the mass of the active material and ΔV is the voltage scan range.

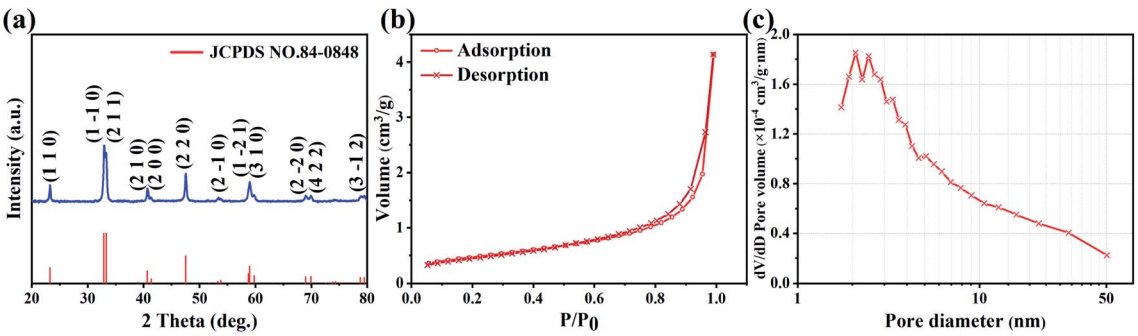

Fig. 1 (a) XRD pattern, (b) N_2 sorption isotherm and (c) BJH pore size distribution curve of $LaCoO_3$ powders.

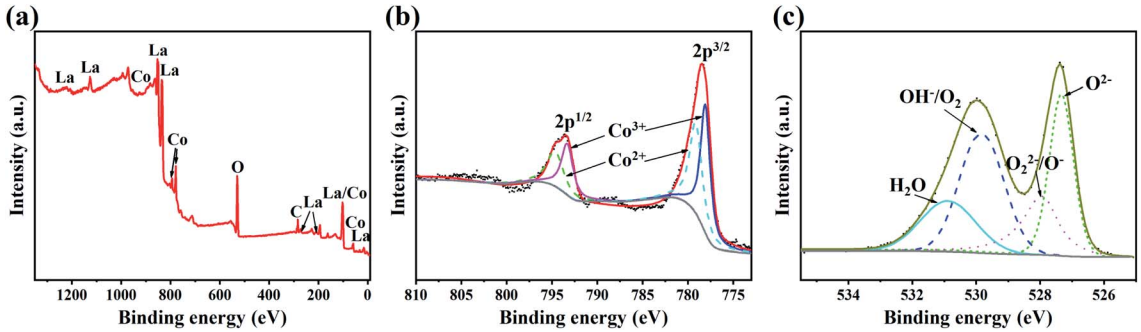

Fig. 2 (a) XPS spectrum, (b) Co 2p XPS spectra and (c) O 1s XPS spectra of $LaCoO_3$.

Table 1 Binding energy and relative area of Co^{2+}/Co^{3+} at $2p_{3/2}$

Co^{2+}		Co^{3+}		
Binding energy (eV)	Relative area (%)	Binding energy (eV)	Relative area (%)	Co^{2+}/Co^{3+}
779.2	47.69	778.1	52.31	0.92

3. Results and discussion

3.1 Structural and morphological analysis

Fig. 1(a) shows the XRD patterns of prepared $LaCoO_3$ samples, which characterizes the crystal structure and phase composition of the samples. As observed from the XRD patterns, the samples display the diffraction peaks at $2\theta = 23.2°$, 32.9°, 33.3°, 40.7°, 41.3°, 47.5°, 53.4°, 59.0°, 59.7°, 69.0°, 69.9°, 78.8°, corresponding to the (110), (1–10), (211), (210), (200), (220), (2–10), (1–21), (310), (2–20), (422) and (3–12) planes respectively. The patterns are well matched with the standard card (JCPDS no. 84-0848) of rhombohedral perovskite structure $LaCoO_3$ and there are no impurity obvious peaks corresponding to other phases, which indicates that the prepared samples are single phase $LaCoO_3$ powders. And the micro morphology of samples is shown as nanoparticles with irregular surface with a size of 30–100 nm.[43]

The BET specific surface area and pore size distribution can be obtained by N_2 adsorption/desorption experiments. Fig. 1(b) shows the N_2 adsorption–desorption isotherm of the samples. As shown in the figure, a type-IV isotherm with a H3 hysteresis loop is observed. The type-IV isotherm demonstrates the presence of mesoporous structures, while the H3 hysteresis loop has no obvious saturated adsorption platform, indicating that the pore structure is irregular. The calculated BET specific surface area value is 2.70 $m^2\ g^{-1}$. The pore size distribution assessed by Barrett–Joyner–Halenda (BJH) methods is illustrated in Fig. 1(c). The results reveal that the pore size distribution is mainly in the range of 1.7–50 nm, and the average pore diameter is 17.27 nm. The pore size can affect its performance and stability by reducing the charge transfer resistance, enabling fast electron transfer from the electrode and reducing the volume change during charge/discharge cycles.[45–48] The N_2 adsorption–desorption isotherm and corresponding pore size distribution indicate that the mesoporous structure of the samples is uniformly stacked.

The XPS spectra of the $LaCoO_3$ samples are shown in Fig. 2. According to these spectra, the species and existing states of the elements are analyzed. Fig. 2(a) shows the XPS full spectrum with binding energy ranging from 200 to 1200 eV, indicating the presence of only four elements of La, Co, O, C. And C is the adsorbed carbon used for charge correction. Fig. 2(b) shows the Co 2p XPS spectra of the samples, revealing two spin–orbit peaks of $2p_{1/2}$ and $2p_{3/2}$ around 793.6 eV and 778.4 eV. By fitting the two peaks, the characteristic peaks of Co^{2+} at 794.7 eV ($2p_{1/2}$) and 779.2 eV ($2p_{3/2}$), and the characteristic peaks of Co^{3+} at 793.4 eV ($2p_{1/2}$) and 778.1 eV ($2p_{3/2}$) are obtained. The atomic ratio of Co^{2+}/Co^{3+} can be obtained by comparing the areas covered by the fitted curve. The peak fitting results at $2p_{3/2}$ are shown in Table 1. The atomic ratio of Co^{2+}/Co^{3+} in the samples is 0.92. Fig. 2(c) shows the O 1 s XPS spectra of the samples, which can be divided into four characteristic peaks: lattice oxygen species (O^{2-}) at 527.3 eV, surface adsorbed oxygen species (O_2^{2-}/O^-) at 527.9 eV, hydroxyl (OH^-) or surface-adsorbed O_2 at 530.3 eV, and H_2O at 530.9 eV. The relative content of each oxygen species in terms of relative area is shown in Table 2. The amount of adsorbed oxygen is closely associated with the oxygen vacancies.[49] It means that the content of oxygen vacancies in the sample is 18.1%.

Table 2 Binding energy and relative content of O 1s

Species	Binding energy (eV)	Relative content (%)
O^{2-}	527.3	30.26
O_2^{2-}/O^-	527.9	18.09
OH^-/O_2	529.9	32.89
H_2O	530.9	18.76

3.2 Electrochemical measurements

3.2.1 Effect of potential window. The energy storage mechanism of $LaCoO_3$ electrode in the KOH electrolyte is oxygen ion intercalation mediated through oxidation of cobalt centers.[16,50] The equation is as follows,[43]

$$La[Co_{2\delta}^{2+}, Co_{1-2\delta}^{3+}]O_{3-\delta} + 2\delta OH^- = LaCo^{3+}O_3 + 2\delta e^- + \delta H_2O \quad (2)$$

$$LaCo^{3+}O_3 + 2\delta OH^- = La[Co_{2\delta}^{4+}, Co_{1-2\delta}^{3+}]O_{3+\delta} + 2\delta e^- + \delta H_2O \quad (3)$$

In the reaction described in eqn (2), OH^- is adsorbed on surface to generate O^{2-} and H_2O, then O^{2-} diffuse along octahedral edges to fill in the oxygen vacancies and form the lattice oxygen species; meanwhile, Co^{2+} is oxidized to Co^{3+}. Then in the reaction described in eqn (3), excess adsorbed OH^- is intercalated on the surface forming the adsorbed oxygen species and further oxidize partial Co^{3+} to Co^{4+}.

In order to investigate the effect of different potential windows on the performance degradation of $LaCoO_3$//$LaCoO_3$ symmetrical supercapacitors, cyclic charge–discharge test of 500 cycles where the maximum voltage is varied from 1.0 V to 1.6 V is carried out in a two-electrode system at current density of 1 A g^{-1}. Fig. 3(a) shows the variation of capacitance retention with cycle number under different potential windows. The capacitance retention first decreases rapidly and then slowly with the increase in number of cycles, and it decrease faster and more under higher potential window. The inset shows that the capacitance retention changes periodically in the last fifty cycles. Fig. 3(b) shows that the specific capacitance before and after cycling test and capacitance retention changes with increasing potential window. The specific capacitance increases with increasing potential window. Meanwhile the difference between specific capacitance increases with increasing potential window, and the capacitance retention decreases from 98.2% with the potential window of 0–1.0 V to 87.1% with the potential window of 0–1.5 V. Variance is a statistical characteristic that describe the degree of data dispersion. Referring to the relevant literature of electrochemical research,[51] variance is used to evaluate the fluctuation degree of specific capacitance and coulomb efficiency in this work. Fig. 3(c) shows that the variance of specific capacitance remains low when the maximum voltage is less than 1.3 V, then it increases sharply when the maximum voltage reaches 1.4 V and 1.5 V. Fig. 3(d) shows that the average of coulombic efficiency decreases from 97.8% with the potential window of 0–1.0 V to 89.2% with the potential window of 0–1.5 V, in addition, it decreases rapidly when the maximum voltage reaches 1.4 V and 1.5 V. And the variance of coulombic efficiency increases in fluctuation with increasing potential window. The change of coulomb efficiency indicates that the reversibility and stability of charge and discharge process decrease. The results of this test reveal that increasing potential window makes the degradation of the supercapacitors more intense and the stability worse.

The CV curves and GCD curves under different potential windows before the cyclic charge–discharge test are shown in Fig. 4. The scan rate of the CV test is 10 mV s^{-1}, and the current density of the GCD test is 1 A g^{-1}. It can be seen from Fig. 4(a) that the CV curves are rectangular, which demonstrate the capacitance characteristics of supercapacitor energy storage. There are two pairs of redox peaks at about 0.3 V and 0.75 V in

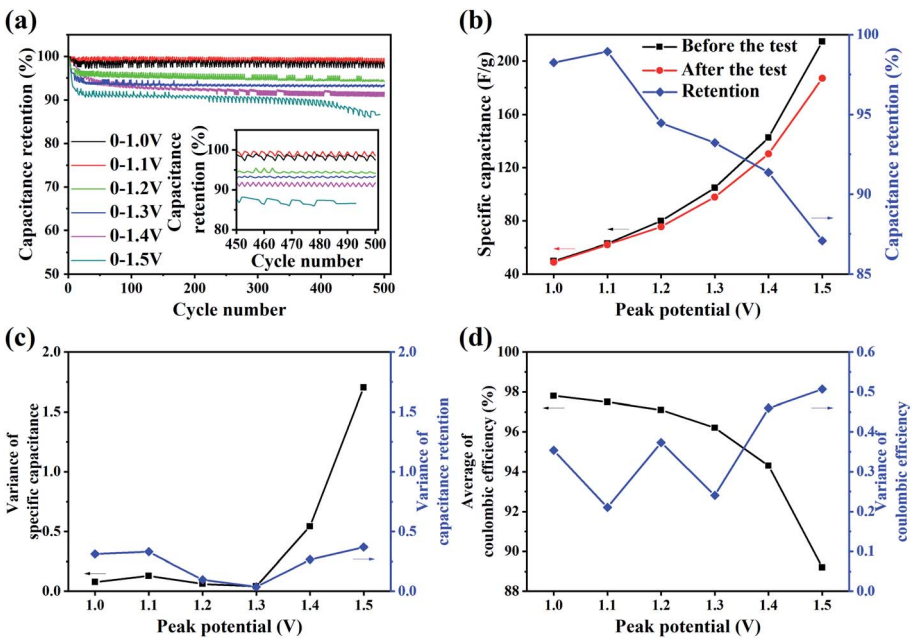

Fig. 3 Cycling performance of $LaCoO_3$//$LaCoO_3$ SC under different potential windows. (a) Capacitance retention changed with cycle number; inset: variation in the last 50 cycles. (b) Comparison of specific capacitance before and after cycling test and capacitance retention, (c) variance of specific capacitance and capacitance retention, (d) average and variance of coulombic efficiency changed with different peak potentials.

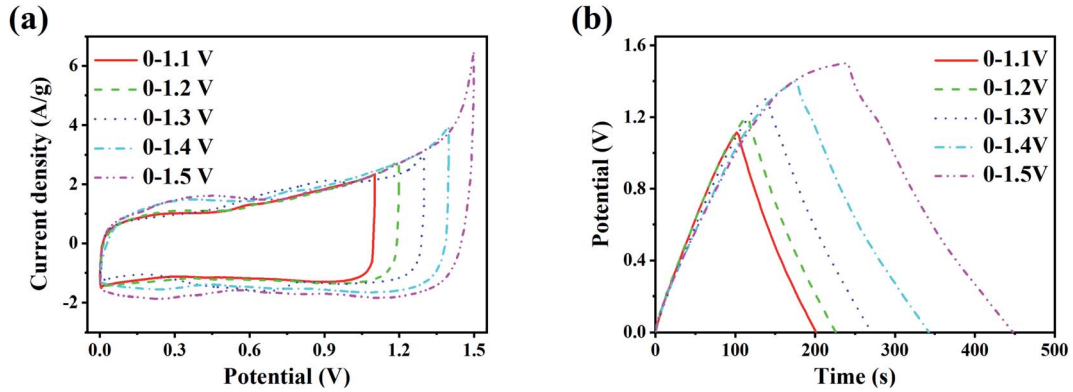

Fig. 4 (a) CV curves and (b) GCD curves of $LaCoO_3$//$LaCoO_3$ SC under different potential windows.

the CV curve under each potential window, which corresponds to the pseudocapacitive reaction of $LaCoO_3$. Besides, the redox peaks become more prominent with increasing potential window, and the polarization of the CV curve intensifies. When the maximum voltage reaches 1.5 V, the polarization of the CV curve is already very intense, leading to the loss of good cycling performance. As shown in Fig. 4(b), the GCD curves are triangular. With increasing potential window, the GCD curve gradually appears a potential stagnation platform near the maximum voltage, and the coulomb efficiency decreases, indicating that the reversibility of the charge and discharge process decreases under increased potential window.

3.2.2 Effect of current density. To investigate the effect of different current densities on the performance degradation of the supercapacitors, cyclic charge–discharge test of 500 cycles is carried out with changing current density in the two-electrode system. The current density of the test is 1 A g^{-1}, 2 A g^{-1}, 4 A g^{-1}, 6 A g^{-1}, 8 A g^{-1} and 10 A g^{-1}, and the potential window of the test is 0–1.4 V. Fig. 5(a) shows the variation of capacitance retention with cycle number at different current densities.

It can be seen that the capacitance retention decreases in fluctuation with increase in number of cycles. Moreover, the capacitance retention decreases faster and more and the fluctuation of it is greater when the current density is higher. The

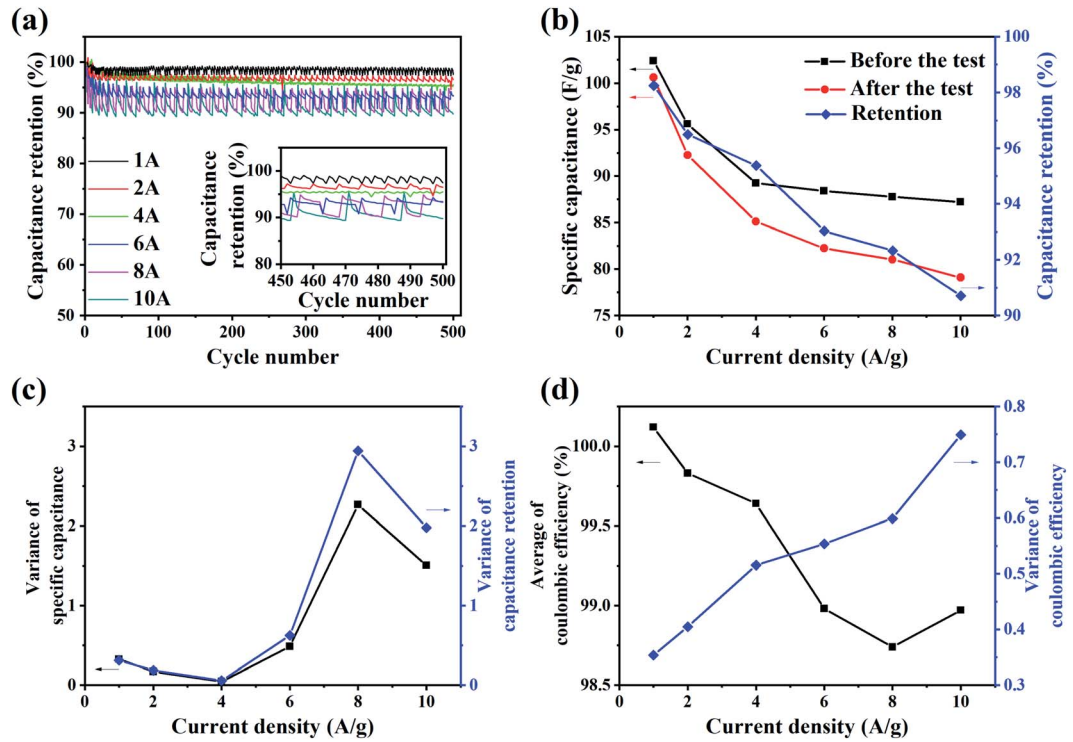

Fig. 5 Cycling performance of $LaCoO_3$//$LaCoO_3$ SC at different current densities. (a) Capacitance retention changed with cycle number; inset: variation in the last 50 cycles. (b) Comparison of specific capacitance before and after cycling test and capacitance retention, (c) variance of specific capacitance and capacitance retention, (d) average and variance of coulombic efficiency changed with different peak potentials.

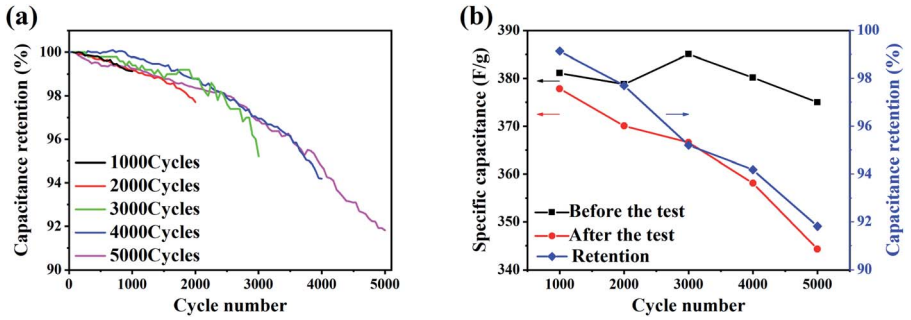

Fig. 6 (a) Specific capacitance of $LaCoO_3$//$LaCoO_3$ SC changed with cycle number at a current density of 1 A g^{-1} under potential window of 0–1.4 V. (b) Comparison of specific capacitance of electrode before and after the cycling test with different cycle number.

inset shows that the capacitance retention changes periodically in the last fifty cycles. Fig. 5(b) shows that the specific capacitance and the capacitance retention decrease with the increase of current density. The rate of change also decreases with the increase of current density. This is in line with the general law of the rate performance of energy storage devices. Fig. 5(c) shows that the variance of specific capacitance and capacitance retention increases with the increase of current density, indicating that the fluctuation of the specific capacitance is greater with the increase of current density. Fig. 5(d) shows that the average of coulombic efficiency decreases and the variance of coulombic efficiency increases, which indicates that reversibility and stability of charge and discharge process decrease with the increase of current density. According to this test, the increase of current density has a negative effect on the stability of the supercapacitors.

3.2.3 Effect of number of cycles. Cyclic charge–discharge test of different cycles is carried out in the two-electrode system under the potential window of 0–1.4 V at current density of 1 A g^{-1} 1000, 2000, 3000, 4000, 5000 cycles are carried out respectively. Fig. 6(a) shows the variation of specific capacitance with cycle number. In order to clearly show the variation trend of the specific capacitance of each test, the curves are translated, so the ordinate in the figure has no practical significance. Fig. 6(b) shows the curve of the specific capacitance of electrode before and after the test with respect to the number of cycles, as well as the curve of the capacitance retention. The capacitance retention is 98.9% after 1000 cycles and 90.5% after 5000 cycles.

Table 3 Intensity of redox peaks in CV curves with different number of cycles

Number of cycles	I_1 (A g^{-1})	I_2 (A g^{-1})	I_1/I_2
1000	2.051	2.440	0.841
2000	1.907	2.373	0.804
3000	1.875	2.346	0.799
4000	1.723	2.354	0.732
5000	1.056	2.191	0.482

As shown in Fig. 6, the specific capacitance decreases linearly with the increase in number of cycles. The curve of capacitance retention with respect to the number of cycles also decreases linearly. It indicates that the degradation is a gradual process.

The CV test and GCD test are carried out in the three-electrode system for the $LaCoO_3$ electrodes after the cycling tests. The scan rate of CV test is 10 mV s^{-1}, the current density of GCD test is 1 A g^{-1}, and the potential window of both tests is −0.3–0.5 V. Fig. 7(a) shows the CV curves of the electrodes after each cycling test. There are two pairs of redox peaks at about 0.026 V and 0.218 V, which shows the pseudocapacitive electrochemical features. The intensity of redox peaks is shown in Table 3. I_1 is the intensity of the redox peak at low potential (about 0.026 V), and I_2 is the intensity of the redox peak at high potential (about 0.218 V). As the number of cycles increases, the intensity ratio I_1/I_2 gradually decreases. The ratio after 1000 and

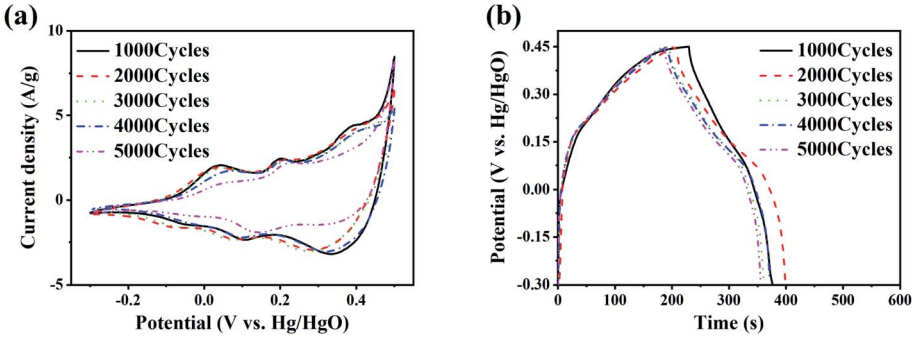

Fig. 7 (a) CV curves and (b) GCD curves of $LaCoO_3$ electrodes with different cycle number.

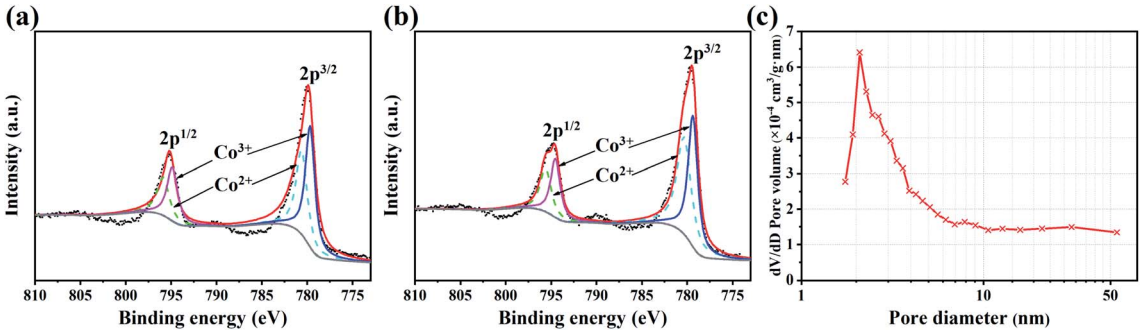

Fig. 8 Co 2p XPS spectra of $LaCoO_3$ after (a) 4000 and (b) 5000 cycles. (c) BJH pore size distribution curve of $LaCoO_3$ after 1000 cycles.

5000 cycles are 0.841 and 0.482, respectively. It indicates that the reaction in eqn (2) is relatively weakened, and the reaction in eqn (3) is relatively enhanced. Fig. 7(b) shows the GCD curves of the electrodes after each test. It can be seen that the charge and discharge time of the electrodes with more cycles is shortened.

To study the change in chemical composition of the electrode surface active material after the cycling test, the $LaCoO_3$, which is obtained from the electrodes after 4000 and 5000 cycles, is tested by XPS. Fig. 8(a) and Fig. 8(b) shows the XPS spectra of $LaCoO_3$ after 4000 and 5000 cycles. Table 4 shows the peak fitting results of Co elements at $2p_{3/2}$ with the number of cycles of 0, 4000 and 5000. It can be seen that the atomic ratio of Co^{2+}/Co^{3+} is 0.92 before the cycling test, and decreases to 0.84 after 4000 cycles, and 0.70 after 5000 cycles.

Pseudocapacitive materials store and release charges through highly reversible redox reactions or ion intercalation/deintercalation. The key factor influencing the performance of storing and releasing charges is the number of oxygen vacancies in the active material.[52] Then in the $LaCoO_3$ samples with a certain total amount of Co elements, higher Co^{2+} content indicates more oxygen vacancies and leads to better energy storage performance. Considering the decreasing trend of intensity ratio I_1/I_2 of redox peaks with the increase of the number of cycles, it can be concluded that the change in the valence state of Co elements in the cycling test leads to the degradation. The Co elements in the $LaCoO_3$ crystal changes to a higher valence state (Co^{3+} or Co^{4+}), resulting in a decrease in the content of Co^{2+} and the number of oxygen vacancies, which ultimately makes the electrochemical performance of the $LaCoO_3$ electrode decreased.

Table 5 OH^- concentration of electrolyte with different number of cycles

Number of cycles	Concentration (mol L^{-1})
0	5.79
5000	5.37

Fig. 8(c) shows the pore size distribution of the active material after 1000 cycles, calculated by the BJH method. As shown in the figure, the pore size distribution of the material after cycling is still mainly in the range of 1.7–50 nm, with the average pore diameter increasing to 22.32 nm. The increase in pore size slows down the performance degradation of electrode to some extent, that is, the capacitance retention curve tends to be flat during the cycling test.

Besides, the electrolyte consumption in the cycling test is studied. The prepared 6 mol L^{-1} KOH solution is divided into two groups. One is used for the cycling test as the electrolyte, and the other is used as the reference group. After the cycling test, the OH^- concentration of the two groups of KOH solution is measured. Since the pH values of the two groups of samples are both too large (greater than 14), the OH^- concentration is measured by dilution titration method at the ambient temperature of 13 °C. The measurement results are shown in Table 5. The OH^- concentration of the reference group was 5.79 mol L^{-1}, and the OH^- concentration of the solution after the cycling test was 5.37 mol L^{-1}. It can be seen that the concentration of OH^- in the electrolyte decreases significantly after the cycling test. While the Faraday redox reaction that occurs on the surface of the $LaCoO_3$ electrode should be highly

Table 4 Binding energy and relative area of Co^{2+} and Co^{3+} at $2p_{3/2}$ with different number of cycles

	Co^{2+}		Co^{3+}		
Number of cycles	Binding energy (eV)	Relative area (%)	Binding energy (eV)	Relative area (%)	Co^{2+}/Co^{3+}
0	794.68	47.69	793.38	52.31	0.92
4000	794.67	45.65	793.38	54.35	0.84
5000	794.70	41.18	793.37	58.82	0.70

reversible, the progress of the reaction should not consume OH^- in the electrolyte ideally. It can be inferred that the degradation mechanism of the supercapacitor is that OH^- participates in an irreversible reaction during the cycles, which leads to a decrease in the ratio of Co^{2+}/Co^{3+} and the number of oxygen vacancies, and ultimately leads to the performance degradation of $LaCoO_3$ electrodes.

4. Conclusions

In this paper, $LaCoO_3$ powders were synthesized by the urea combustion method and the corresponding supercapacitor was prepared. By analyzing the effect of charge and discharge potential window, current density and number of cycles on the cycle stability of $LaCoO_3$//$LaCoO_3$ symmetric supercapacitors, the main conclusions obtained are as follows:

(1) The increase of the potential window can improve the specific capacitance performance of $LaCoO_3$//$LaCoO_3$ symmetrical supercapacitors, while the increase of current density reduces the specific capacitance performance. However, the increase of potential window and current density will decrease the capacitance retention and coulombic efficiency of $LaCoO_3$//$LaCoO_3$ symmetrical supercapacitors.

(2) The increase of the number of cycles makes the capacitance retention of $LaCoO_3$//$LaCoO_3$ symmetrical supercapacitors continue to decrease, and the intensity ratio I_1/I_2 of redox peaks in the CV curves of the $LaCoO_3$ electrode after the cycling test also shows a downward trend. XPS results show that the ratio of Co^{2+}/Co^{3+} decreases with the increase of the number of cycles, meaning that the oxygen vacancies decrease. Through comparing the OH^- concentration in the KOH electrolyte before and after 5000 cycles, it was found that the OH^- concentration decreased significantly after the cycling test, indicating that OH^- participated in the irreversible reaction. In summary, there are irreversible reactions occurring and accumulating during the cycles, which makes Co^{2+} in $LaCoO_3$ gradually transform to Co^{3+} or even higher valence states, reduces the Co^{2+}/Co^{3+} ratio in $LaCoO_3$ and the number of oxygen vacancies, and ultimately leads to performance degradation.

Conflicts of interest

The authors declare that they have no known competing financial interests or personal relationships that could have appeared to influence the work reported in this paper.

Acknowledgements

The authors are grateful for support by the 111 Project (B17034), the Innovative Research Team Development Program of Ministry of Education of China (IRT_17R83) and the Hubei Superior and Distinctive Discipline Group of "Mechatronics and Automobiles" (No. XKQ2021001). The Center of Material XRD, BET and XPS examinations were assisted by the Center of Material Research and Analysis of Wuhan University of Technology.

References

1 B. E. Conway, *Electrochemical Supercapacitors: Scientific Fundamentals and Technological Applications*, Springer Science + Business Media, New York, 1999.
2 B. Fang, A. Bonakdarpour, M. S. Kim, *et al.*, *Microporous Mesoporous Mater.*, 2013, **182**, 1–7.
3 Z. Lin, S. Shen, Z. Wang, *et al.*, *Iscience*, 2021, 102469.
4 Q. Zhang and G. Li, *IEEE Trans. Power Electron.*, 2020, **35**(1), 1014–1021.
5 B. Yang, J. Wang, X. Zhang, J. Wang, H. Shu, S. Li, T. He, C. Lan and T. Yu, *J. Power Sources*, 2020, **448**, 227444.
6 Z. Song, J. Li, J. Hou, H. Hofmann, M. Ouyang and J. Du, *Energy*, 2018, **154**, 433–441.
7 H. Li, J. Peng, J. He, R. Zhou, Z. Huang and J. Pan, *IEEE Trans. Control Syst. Technol.*, 2018, **26**(4), 1219–1232.
8 L. Di-Noia, F. Genduso, R. Miceli and R. Rizzo, *IEEE Trans. Ind. Appl.*, 2019, **55**(1), 794–801.
9 G. Ren, J. Liu, J. Wan, Y. Guo and D. Yu, *Appl. Energy*, 2017, **204**, 47–65.
10 W. Jing, C. Lai, S. Wong and M. Wong, *IET Renew. Power Gener.*, 2017, **11**(4), 461–469.
11 M. Masaki, L. Zhang and X. Xia, *Appl. Energy*, 2019, **242**, 393–402.
12 B. Fang and L. Binder, *J. Phys. Chem. B*, 2006, **110**(15), 7877–7882.
13 Y. Ma, Y. Guo, C. Zhou, *et al.*, *Electrochim. Acta*, 2016, **210**, 897–904.
14 A. Bazan-Aguilar, M. Ponce-Vargas, C. Caycho, A. Rosa-Toro and A. Moncada, *ACS Omega*, 2020, **5**(50), 32149–32159.
15 B. Fang, Y. Z. Wei and M. Kumagai, *J. Power Sources*, 2006, **155**(2), 487–491.
16 J. Mefford, W. Hardin and S. Dai, *Nat. Mater.*, 2014, **13**(7), 726–732.
17 B. Fang, Y. Z. Wei, K. Suzuki, *et al.*, *Electrochim. Acta*, 2005, **50**(18), 3616–3621.
18 D. Wang, Y. Xiao, X. Luo, *et al.*, *ACS Sustainable Chem. Eng.*, 2017, **5**(3), 2509–2515.
19 S. Shen, Z. Lin, K. Song, *et al.*, *Angew. Chem., Int. Ed.*, 2021, **60**(22), 12360–12365.
20 W. Zhong, B. Xiao, Z. Lin, *et al.*, *Adv. Mater.*, 2021, **33**(9), 2007894.
21 Z. Wang, Z. Lin, J. Deng, *et al.*, *Adv. Energy Mater.*, 2021, **11**(5), 2170020.
22 W. Zhong, Z. Wang, N. Gao, *et al.*, *Angew. Chem., Int. Ed.*, 2020, **59**(50), 22743–22748.
23 T. Liu and Y. Li, *InfoMat*, 2020, **2**(5), 807–842.
24 J. Mefford, W. Hardin and S. Dai, *Nat. Mater.*, 2014, **13**(7), 726–732.
25 W. Che, M. Wei, Z. Sang, K. Ouyang, Y. Liu and J. Liu, *J. Alloys Compd.*, 2018, **731**, 381–388.
26 Z. Li, W. Zhang, C. Yuan and Y. Su, *RSC Adv.*, 2017, **7**, 12931–12937.
27 Y. Cao, B. Lin, Y. Sun, Y. Hong and X. Zhang, *J. Alloys Compd.*, 2015, **638**, 204–213.
28 Z. Li, W. Zhang, H. Wang and B. Yang, *Electrochim. Acta*, 2017, **258**, 561–570.

29 S. Yin, Y. Wu, J. Chen, Z. Chen, H. Hou, Q. Liu, Y. Wang and W. Zhang, *Funct. Mater. Lett.*, 2018, **11**(1), 1850013–1850016.
30 Z. Elsiddig, H. Xu, D. Wang, W. Zhang, X. Guo, Y. Zhang, Z. Sun and J. Chen, *Electrochim. Acta*, 2017, **253**, 422–429.
31 Z. Elsiddig, D. Wang, H. Xu, W. Zhang, T. Zhang, P. Zhang, W. Tian, Z. Sun and J. Chen, *J. Alloys Compd.*, 2018, **740**, 148–155.
32 Y. Song, Z. Wang, Y. Yan, M. Zhang, G. Wang, T. Yin, Y. Xue, G. Fan and Q. Min, *J. Energy Chem.*, 2020, **43**, 173–181.
33 Y. Guo, *Int. J. Electrochem. Sci.*, 2017, **12**, 7121–7127.
34 D. Weingarth, A. Foelske-Schmitz and R. Kötz, *J. Power Sources*, 2013, **225**, 84–88.
35 D. Weingarth, H. Noh, A. Foelske-Schmitz, A. Wokaun and R. Kötz, *Electrochim. Acta*, 2013, **103**, 119–124.
36 N. Wang, Q. Zhang, P. Zhao, M. Yao, W. Hu and S. Komarneni, *Ceram. Int.*, 2017, **43**(7), 5687–5692.
37 L. He, Y. Shu, W. Li and M. Liu, *J. Mater. Sci.: Mater. Electron.*, 2019, **30**(1), 17–25.
38 W. Lajnef, J. Vinassa, O. Briat, H. Brouji, S. Azzopardi and E. Woirgard, *IET Electr. Power Appl.*, 2007, **1**(5), 683–689.
39 H. Brouji, O. Briat, J. Vinassa, N. Bertrand and E. Woirgard, *IEEE Trans. Veh. Technol.*, 2009, **58**(8), 3917–3929.
40 S. Liu, L. Wei and H. Wang, *Appl. Energy*, 2020, **278**, 115436.
41 C. Julien and A. Mauger, *Nanomaterials*, 2017, **7**(11), 396.
42 Y. Shao, M. Kady, J. Sun, Y. Li, Q. Zhang, M. Zhu, H. Wang, B. Dunn and R. Kaner, *Chem. Rev.*, 2018, **118**, 9233–9280.
43 G. Guo, K. Ouyang, J. Yu, Y. Liu, S. Feng and M. Wei, *ACS Appl. Energy Mater.*, 2019, **3**(1), 300–308.
44 D. Singh, N. Choudhary and A. Mahajan, *Ionics*, 2015, **21**, 1031–1037.
45 B. Fang, J. Kim, M. Kim and J. Yu, *Acc. Chem. Res.*, 2013, **46**, 1397–1406.
46 Y. Xing, B. Fang, A. Bonakdarpour, *et al.*, *Int. J. Hydrogen Energy*, 2014, **39**(15), 7859–7867.
47 Y. J. Wang, B. Fang, H. Li, *et al.*, *Prog. Mater. Sci.*, 2016, **82**, 445–498.
48 W. B. Hua, X. D. Guo, Z. Zheng, *et al.*, *J. Power Sources*, 2015, **275**, 200–206.
49 N. Arjun, G. Pan and T. Yang, *Results Phys.*, 2017, **7**, 920–926.
50 L. Zhu, Y. Liu, C. Su, W. Zhou, M. Liu and Z. Shao, *Angew. Chem., Int. Ed.*, 2016, **55**(33), 9576–9579.
51 X. Yuan, L. Li, H. Gou, *et al.*, *Appl. Energy*, 2015, **157**, 75–84.
52 Y. A. Nemudry, E. Goldberg, M. Aguirre and M. Alario-Franco, *Solid State Sci.*, 2002, **4**(5), 677–690.